PREDICTING THE ONSET OF FLOW UNSTEADINESS BASED ON STABILITY ANALYSIS

J.D. Crouch
Boeing Commercial Airplanes, Seattle, WA, USA

A. Garbaruk, D. Magidov
Saint-Petersburg State Polytechnic University, St.-Petersburg, Russia

Abstract

Global stability theory is used to predict the onset of unsteadiness as a perturbation to a steady RANS solution. Results are presented for the onset of vortex shedding and the onset of transonic buffet. The results are shown to be in good agreement with experiments and unsteady RANS calculations.

1. Introduction

A reliable prediction for the onset of natural flow unsteadiness is of significant importance for many aerodynamic applications. The most rigorous numerical approach to such problems is Direct Numerical Simulation (DNS), i.e., time-accurate integration of the Navier-Stokes equations. However this approach is far from affordable for turbulent flows at practically meaningful high Reynolds numbers. For this reason, currently such flows can only be treated with the use of Large Eddy Simulation (LES), Unsteady Reynolds Averaged Navier-Stokes equations (URANS), or with hybrid approaches, such as Detached-Eddy Simulation (DES). However the use of LES, even for statistically stationary wall-bounded flows, is also severely restricted by *Re* number. Application of DES enables simulation of high *Re* number flows, but is not applicable to the attached flows or those with shallow separation. Thus, URANS is currently the principal approach used for evaluation of the attached or mildly-separated turbulent flows inclined to large-scale quasi-periodic oscillations.

Leaving aside the theoretical background for the URANS approach [1], its practical application implies time-accurate integration of the RANS equations over a wide range of control parameters (angle of attack, Reynolds number, Mach number). A large number of computations are required to define the boundary between steady and unsteady solutions in this “design space”. Not only would such an exercise have very high computational cost, but its output might be rather vague since getting an unsteady solution of the RANS equations is a subtle procedure that depends upon the grid,

the numerical method, and the way in which the flow is initialized.

Prediction of the onset of global turbulent-flow unsteadiness based on the classical linear stability theory offers a very attractive alternative to the URANS-based approach. However its implementation is far from trivial as well, and demands the resolution of a number of computational issues associated with both numerical solution of the background steady flow and the associated matrix eigenvalue problem.

In the present work, an appropriately efficient numerical procedure for both these stages is developed with the final outcome being a set of eigenvalues and corresponding eigenvectors of the perturbation matrix. The developed methodology is tested on a set of flows including the laminar flow over a circular cylinder and turbulent transonic flows over biconvex and NACA 0012 airfoils. In all these cases, it provides good agreement with the available experimental data and with corresponding URANS results obtained in the present study and published in the literature.

2. Theoretical formulation

We consider the two-dimensional compressible unsteady flow governed by the URANS equations with the Spalart-Allmaras (SA) turbulence model [2] used to provide closure for the Reynolds stresses. This leads to a set of five equations: continuity, streamwise and transverse momentum, energy, and eddy viscosity. These equations can be written in terms of the primitive variables, $q = \{\rho, u, v, T, \nu_t\}$ in the following homogeneous vector form:

$$R(q)\frac{\partial q}{\partial t} + N(q) = 0 \qquad (1)$$

Here ρ is the density, T is the temperature, u and v are velocities in the x, y directions, respectively, and ν_t is the eddy viscosity.

The state vector describing the total flow field can be decomposed into a steady-state $\bar{q} = \{\bar{\rho}, \bar{u}, \bar{v}, \bar{T}, \bar{\nu}_t\}$ and an unsteady vector $q' = \{\rho', u', v', T', \nu_t'\}$, $q = \bar{q} + q'$. The vector $\bar{q}$ is a solution of the steady form of the system (1) - that is with $\partial\bar{q}/\partial t \equiv 0$.

For conditions close to steady state, the unsteady component q' can be considered as a small perturbation to the vector $\bar{q}$. Substituting $q = \bar{q} + q'$ into equations (1), canceling the terms governing $\bar{q}$, and linearizing the equations in terms of q' yields:

$$\frac{\partial R}{\partial q}\cdot\frac{\partial q'}{\partial t} + \frac{\partial N}{\partial q}\cdot q' = 0 \qquad (2)$$

The linear operator $(\partial R/\partial q)$ contains the terms associated with the time derivatives from the original equations (1). The linear operator $(\partial N/\partial q)$ consists of linear terms from the original equations, and the terms generated by nonlinear interactions between $\bar{q}$ and q'.

The unsteady perturbation to the steady-state flow $\bar{q}(x, y)$ can be represented by time-harmonic normal modes of the form

$$q'(x, y, t) = \hat{q}(x, y)\cdot\exp(-i\omega t). \qquad (3)$$

The function $\hat{q}$ describes the mode shape, and ω is the frequency. In general, both $\hat{q}$ and ω can be complex, so the physical solution is taken as the real part of equation (3).

Substituting (3) into (2) yields a system of equations governing the modal perturbation. Multiplying this system by the matrix $(\partial R/\partial q)^{-1}$ yields the final system of equations for $\hat{q}$ and ω in the form:

$$-i\omega\hat{q} + L(\bar{q})\cdot\hat{q} = 0, \qquad (4)$$

with L being a second-order linear differential operator. Equation (4) with linearized boundary conditions describes an eigenvalue problem, which is solved numerically.

3. Numerical solution

In the present work both steady and time-accurate RANS equations are solved with the use of the NTS code [3] based on an implicit finite-volume formulation on a structured multi-block overlapping grid. The third-order Roe scheme [4] is used for inviscid fluxes, while the viscous momentum and heat fluxes are approximated with the second-order central difference scheme. The convective terms in the eddy-viscosity transport equation of the Spalart-Allmaras model are approximated with the first-order upwind scheme. Time-derivatives are approximated with 2nd-order backward differences (three-layer scheme) with sub-iterations. For the solution of the stability equations (4), the upwind finite-difference approximations are linear.

In order to reduce the numerical dissipation of the upwind differencing we use a "hybrid" scheme which is weighted between upwind and central differencing:

$$\Delta_H = \alpha_H \Delta_{3u} + (1-\alpha_H)\Delta_{4c}, \quad 0 \le \alpha_H \le 1. \quad (5)$$

The finite difference operators Δ_{3u} and Δ_{4c} correspond to the 3-rd order upwind and 4-th order centered schemes, respectively, and α_H is the weighting constant.

To discretize the stability equations, we first introduce a finite-difference grid with the total number of nodes $N_p = N_i \times N_j$. The following one-dimensional ("global") numbering of the grid nodes is used:

$$n = N_j(i-1) + j, \text{ with } n = 1,...,N_p, \quad (6)$$

with $i = 1,...,N_i$, $j = 1,...,N_j$. Now, let the vector $\hat{a}$ with the dimension $N_V = n_{\text{var}} \times N_p$ be the finite-difference analog of the perturbation mode shape ($n_{\text{var}} = 5$ is the number of the primary variables in the RANS equations):

$$\hat{a} = [\hat{q}_{11}, \hat{q}_{12}, ..., \hat{q}_{1N_j}, ..., \hat{q}_{N_iN_j}]^T, \quad (7)$$

or, using global node numbering (6)

$$\hat{a} = [\hat{\rho}_1, \hat{u}_1, \hat{v}_1, \hat{T}_1, \hat{\nu}_{t1}, ..., \hat{\rho}_n, \hat{u}_n, \hat{v}_n, \hat{T}_n, \hat{\nu}_{tn}, ..., \hat{\rho}_{N_p}, \hat{u}_{N_p}, \hat{v}_{N_p}, \hat{T}_{N_p}, \hat{\nu}_{tN_p}]^T. \quad (8)$$

The finite-difference approximation of the system (4) and corresponding linearized boundary conditions can then be presented in the following matrix form:

$$(-i\omega T + S)\cdot \hat{a} = 0, \quad (9)$$

where the matrix S with the dimension N_V is an approximation of the differential operator $L(\bar{q})$ (4), and $\bar{q}$ is the numerical solution of the steady RANS equations on this grid. The specific form of the matrix S depends upon the approximation of the space derivatives in the differential operator. The matrix T in (9) is diagonal ($T_{ml} = 0$ for $m \ne l$); its diagonal elements T_{mm} are equal to 0 for all m corresponding to the boundary points of the computational grid and for all other points $T_{mm} = 1$.

A similar formulation can be used for multi-block grids with global numbering extended to all blocks:

$$n = \sum_{k=1}^{n_b-1} N_p^{(k)} + N_j^{(n_b)}(i-1) + j, \quad (10)$$

with, $i = 1,...,N_i^{(n_b)}$, $j = 1,...,N_j^{(n_b)}$, $n_b = 1,...,N_b$ – block number, and $N_p^{(n_b)} = N_i^{(n_b)} \times N_j^{(n_b)}$.

The eigenvalue problems are solved numerically using the implicitly restarted Arnoldi method [5], which is the member of Krylov subspace projection methods. This method is very efficient for calculating small sets of eigenvalues for large systems.

The eigenvalue problem (9) yields a large number of eigenvalues, but only a small number of these are physically meaningful. We focus on the least-stable eigenmode as an indicator for the onset of unsteadiness. A small number of modes are calculated in the neighborhood of ω^*, where $\mathrm{Im}(\omega^*) > 0$. When necessary, physical modes are distinguished from spurious modes by calculating the average eigenfunction amplitude at the far-field boundary (neglecting the wake region). The physical modes have negligibly small amplitude in the far field compared to the peak modal amplitude.

4. Results

The stability problem formulated in sections 2 and 3 provides a general framework for predicting the onset of unsteadiness for compressible flow including high Reynolds number flows. This approach is now assessed by considering example problems, which serve as limiting cases in terms of their level of complexity. First, we consider vortex shedding for a circular cylinder. This is a low-Reynolds-number laminar-flow condition at an essentially-incompressible Mach number. The other problem considered is transonic buffet onset for a NACA 0012 airfoil and for an 18% thick bi-convex airfoil. This is a high-Reynolds-number turbulent-flow condition, which includes shock waves.

4.1. Vortex-shedding results

Vortex shedding from a circular cylinder at low Reynolds numbers was one of the first problems considered using concepts of global-instability analysis [6, 7, 8]. Meanwhile, this type of approach has been applied to a range of laminar-flow instability problems [9]. We revisit the cylinder problem as a simple test case for the current formulation, and to provide updated estimates for the onset of instability. At low Reynolds numbers the flow is laminar, so the state vector reduces to $\bar{q} = \{\bar{\rho}, \bar{u}, \bar{v}, \bar{T}\}$. The Mach number is taken to be $M = 0.2$.

Contours of u-velocity for the steady flow around the cylinder are shown in Fig. 1, for the Reynolds number $Re = U_\infty D/\nu = 40$. This flow is stable to small unsteady perturbations. However, as the Reynolds number is increased the flow goes unstable – signifying the onset of vortex shedding, with frequency $\mathrm{real}(\omega) = 2\pi f D/U_\infty$.

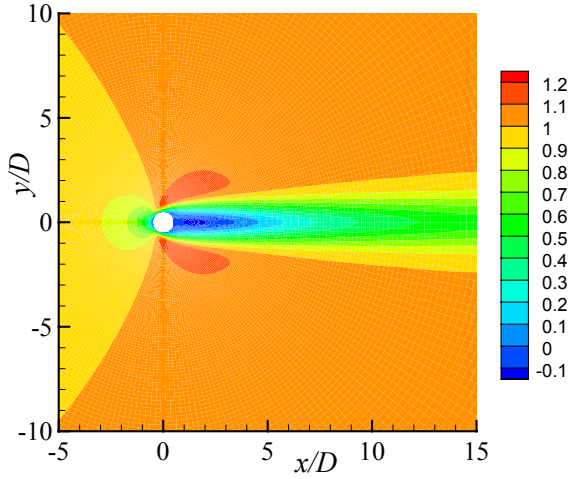

Fig.1: Contours of steady-flow u-velocity.

Table1

Eigenvalues for the circular cylinder with different grids at $M = 0.2$, $Re = 60$.

Grid	Eigenvalue
80×80	0.761137, 0.034922
160×160	0.743282, 0.043301
240×240	0.739835, 0.044272
320×320	0.738708, 0.044557
400×400	0.738223, 0.044679

Table 1 shows the most unstable eigenvalue calculated for $Re = 60$. Results are given for several different grids, ranging from 6,400 points up to 160,000 points. The computational domain for all grids extends to 125 diameters. Results for a significantly larger domain, extending to 200 diameters, turned out virtually the same. The eigenvalues computed on the grid 240×240 are accurate to three significant digits; all subsequent results are based on this grid.

The unsteadiness due to vortex shedding is predicted to occur at $Re = 47$, where $\mathrm{Im}(\omega)$ crosses zero. This is in good agreement with experimental observations of Hammache and Gharib [10] and with the numerical simulations of Barkley and Henderson [11], which give a critical Reynolds number of $Re \approx 46 \pm 1$. The predicted shedding frequency at $Re = 50$ is 0.734, which matches the unsteady results from the NTS code based on the same grid.

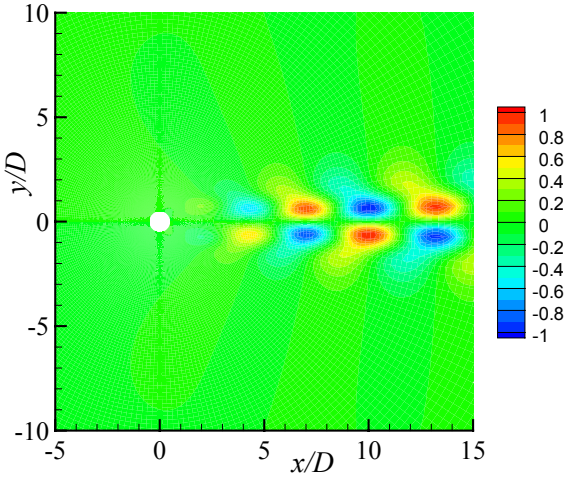

Fig.2: Contours of real($\hat{u}$) for the circular-cylinder unsteady mode.

The mode shape for the least-stable eigenvalue is given in Fig. 2. The figure shows contours of the real part of the *u*-velocity component, real($\hat{u}$). The imaginary part of $\hat{u}$ has the same form as the real part, except the maximum and minimum values occur at the location of the zeros in real($\hat{u}$). When the eigenfunction (with prescribed amplitude) is combined with the mean flow, the total unsteady flow field shows the typical vortex-shedding pattern – as predicted by the time-accurate Navier-Stokes solution at the same *Re*.

4.2. Transonic-buffet results

To examine the potential for predicting transonic-buffet onset using the global stability theory, we consider the NACA 0012 airfoil. This problem was considered earlier in the experiments of McDevitt & Okuno [12] and in the unsteady calculations Barakos & Drikakis [13] and Chung et al. [14]. The transonic flow around a NACA 0012 airfoil at an angle of attack $\alpha > 2^\circ$ exhibits a shockwave on the upper surface. As the angle of attack is increased, the shock intensifies and the flow separates from the airfoil upper surface upstream of the trailing edge. A further increase in the angle of attack results in the forward movement of the separation point from the trailing edge toward the foot of the shock. When the angle of attack exceeds some critical value, the flow becomes globally unsteady. The unsteadiness is characterized by a coupled modulation of the shockwave and the separated shear layer.

The transonic-airfoil calculations are done at relatively high Reynolds numbers, where the boundary layers would typically be turbulent. For these flows the state vector is given by $\bar{q} = \{\bar{\rho}, \bar{u}, \bar{v}, \bar{T}, \bar{\nu}_t\}$. In accordance with the global stability analysis, the critical value for the angle of attack at $M = 0.76$ is 3.05 degrees, which agrees very well with the experimental data [12] and with URANS predictions [14].

Figure 3 shows the steady RANS Mach contours of the flow at $Re = 10^7$, $M = 0.76$ and an angle of attack of 3.2º. The instability mode shape at the same flow conditions is shown in Fig. 4. The perturbation is concentrated around the shock and the boundary layer downstream of the shock. The disturbance maximum at the shock is roughly two orders of

magnitude larger than in the rest of the flow. Qualitatively, the instability represents an oscillation of the shock position. The phase plot shows that as the shock moves downstream, the separated shear layer moves closer to the surface of the airfoil. When the shock moves forward, the shear layer lifts off of the surface. This form of oscillation is in good agreement with the observations of McDevitt & Okuno [12].

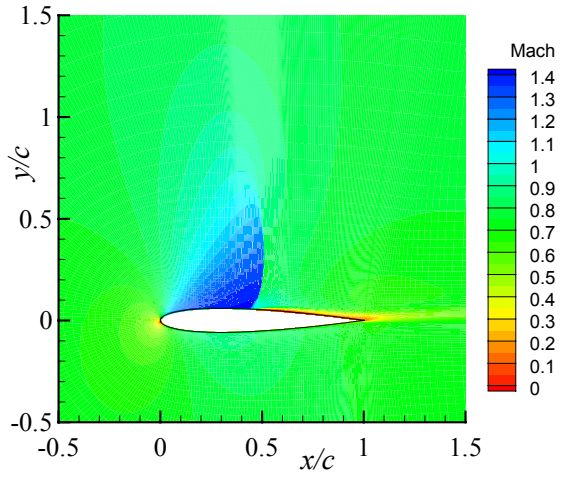

Fig. 3: Contours of steady flow Mach number for the for NACA 0012 airfoil.

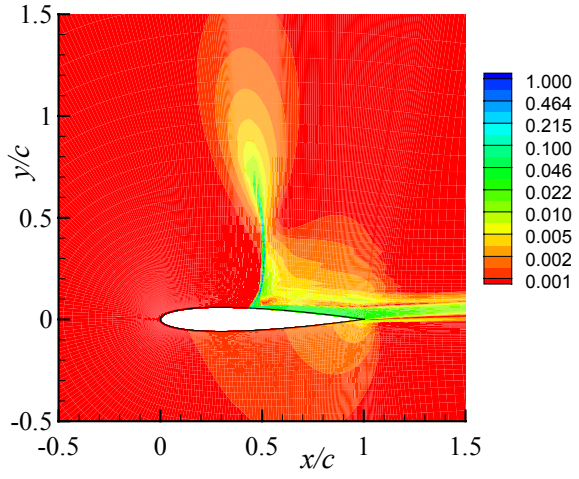

Fig. 4: Contours of $|\hat{u}|$ amplitude for the NACA 0012 unsteady mode.

Another test case for transonic-buffet predictions is the bi-convex airfoil. This problem was considered earlier in the experiments of McDevitt [15] and the unsteady calculations of Rumsey et al. [16]. An 18% thick airfoil is placed in the flow at zero angle of attack. For Mach numbers above $M \approx 0.72$, the flow develops shocks on the upper and lower surfaces. As the Mach number is increased, the shock strength increases as well, and the shock moves toward the trailing edge. The boundary layer begins to separate upstream of the trailing edge. The separation point moves forward with increasing Mach number, reaching the foot of the shock at $M \approx 0.76$.

In the experiments [15] the flow is steady at lower Mach numbers. As the Mach number is increased, the flow goes unsteady at $M \approx 0.76$. The unsteadiness is characterized by large-scale oscillations of the shock – phase-locked to oscillations of the separated shear layer. The unsteadiness persists up to $M \approx 0.78$. When the Mach number is decreased, the unsteadiness persists down to $M \approx 0.73$. The oscillation frequency is nearly uniform over the range of Mach numbers, with $2\pi fc/U_\infty \approx 1$ (or $k = 2\pi f(c/2)/U_\infty \approx 0.5$).

The URANS computations of Rumsey *et al.* [16], performed using the SA turbulence model assuming fully-turbulent flow, show a hysteresis similar to the experiments. As the Mach number is increased in steps of 0.01 the flow goes unsteady between $M = 0.75$ and $M = 0.76$. As the Mach number is decreased, the flow remains unsteady down to $M = 0.73$, and becomes steady at $M = 0.72$.

A comparison of the computations carried out in the present work with those of [16] is shown in Fig. 5. Computations were performed with fully-turbulent boundary-layer flow, as well as, with transition specified at x/c=0.5. Boundary-layer stability calculations suggest that the boundary-layer flow could be laminar back to the shock. One can see that, in general, results obtained in the current work are in good agreement both with experiment [15] and ear-

lier numerical computations [16]. Moreover, as seen from Fig. 5, the results obtained with the imposed transition are much closer to the experimental data.

The global stability analysis for this case (calculated on a half domain with an anti-symmetric boundary condition) also shows good agreement with the experiment and URANS computations – giving the critical Mach number of 0.73.

5. Conclusions

The onset of flow unsteadiness can be predicted using global-stability theory. The approach requires a steady solution of the RANS equations, and an eigenvalue calculation for the unsteady disturbance. Results from this approach are in good agreement with experiments and with unsteady RANS solutions for vortex shedding and for transonic buffet.

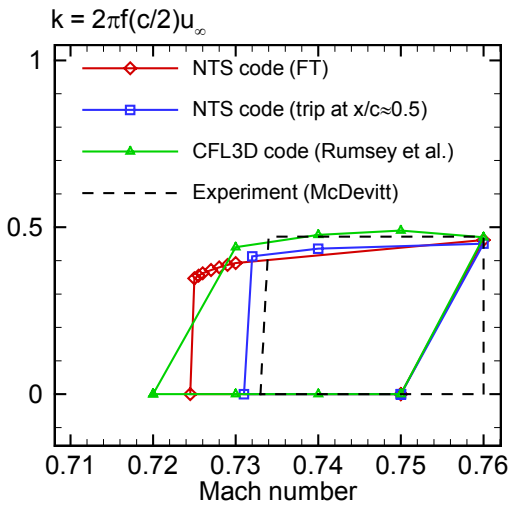

Fig. 5: Frequency variation for 18% bi-convex airfoil.

References

[1] Shur M., Spalart P., Squires K., Strelets M., and Travin A. Persistence and Effects of Three Dimensionality in Unsteady Reynolds-Averaged Navier–Stokes Simulations of Two-Dimensional Bluff Bodies. *AIAA Journal*, Vol 43, accepted for publication in 2005.

[2] Spalart P.R., Allmaras S.R. A One-Equation Turbulence Model for Aerodynamic Flows. *AIAA Paper*, AIAA-92-0439, 1992.

[3] Strelets M., Detached-Eddy Simulation of Massively Separated Flows. *AIAA Paper*, AIAA-2001-0879, 2001.

[4] Roe P. L. Approximate Rieman Solvers, Parameters Vectors and Difference Schemes. *Journal of Computations Phys.*, Vol. 43, pp. 357-378, 1981.

[5] Lehoucq R.B., Sorensen D.C., Yang C. ARPACK user's guide. *SIAM publication*, 1998.

[6] Jackson C. P. A finite-element study of the onset of vortex shedding in flow past variously shaped bodies. *J. Fluid Mech.*, Vol. 182, pp. 23-45, 1987.

[7] Zebib A. Stability of viscous flow past a circular cylinder. *Journal of Engineering Mathematics,* Vol. 21, pp. 155-165, 1987.

[8] Hill D.C. A theoretical approach for analyzing the restabilization of wakes. *AIAA Paper*, AIAA-92-0067, 1992.

[9] Theofilis V. Advances in global linear instability of nonparallel and three-dimensional flows. *Prog. Aero. Sci.*, Vol. 39, pp. 249-315, 2003.

[10] Hammache M., Gharib M. An experimental study of the parallel and oblique vortex shedding from circular cylinders. *J. Fluid Mech.*, Vol. 232, pp. 567-590, 1991.

[11] Barkley D., Henderson R.D. Three-dimensional Floquet stability analysis of the wake of a circular cylinder. *J. Fluid Mech.*, Vol. 322, pp. 215-241, 1996.

[12] McDevitt J., Okuno A.F. Static and dynamic pressure measurements on a NACA 0012 airfoil in the Ames high Reynolds number facility. *NASA-TP-2485*, 1985.

[13] Barakos G., Drikakis D. Numerical simulation of transonic buffet flows using various turbulence closures. *International Journal of Heat and fluid Flow,* Vol. 21, pp. 620-626, 2000.

[14] Chung I., Lee D., Reu T. Prediction of transonic buffet onset for an airfoil with shock induced separation bubble using steady Navier-Stokes solver. *AIAA Paper*, AIAA-2002-2934, 2002.

[15] McDevitt J. Supercritical flow about a thick circular-arc airfoil. *NASA TM-78549*, pp. 1089 -1171, 1979.

[16] Rumsey C.L., Sanetrik M.D., Biedron R.T., Melson N.D., and Parlette E.B. Efficiency and accuracy of time-accurate turbulent Navier-Stokes computations. *Computers and Fluids*, Vol. 25, No. 2, pp. 217-236, 1996.